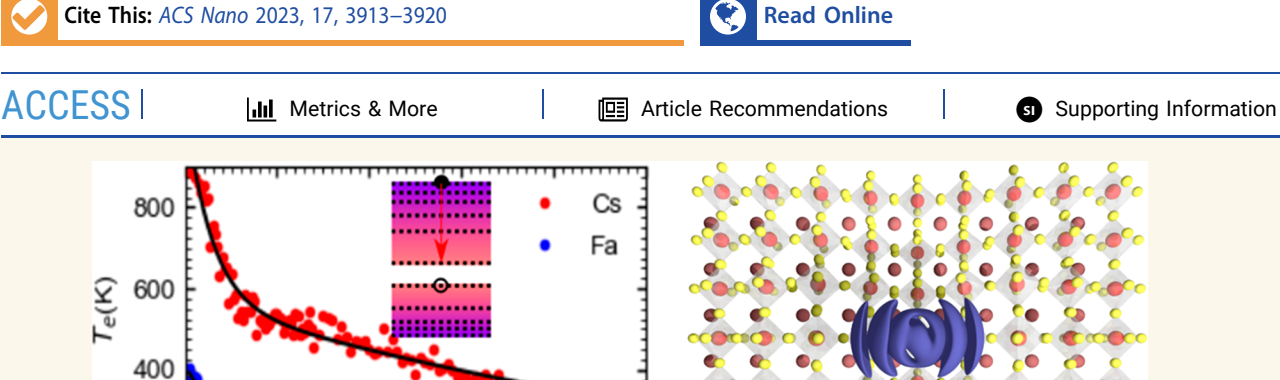
# Breaking Phonon Bottlenecks through Efficient Auger Processes in Perovskite **Nanocrystals**

Harry Baker, Carlos Mora Perez, Colin Sonnichsen, Dallas Strandell, Oleg V. Prezhdo, and Patanjali Kambhampati\*



ABSTRACT: The hot phonon bottleneck has been under intense investigation in perovskites. In the case of perovskite nanocrystals, there may be hot phonon bottlenecks as well as quantum phonon bottlenecks. While they are widely assumed to exist, evidence is growing for the breaking of potential phonon bottlenecks of both forms. Here, we perform state-resolved pump/probe spectroscopy (SRPP) and time-resolved photoluminescence spectroscopy (t-PL) to unravel hot exciton relaxation dynamics in model systems of bulk-like 15 nm nanocrystals of CsPbBr<sub>3</sub> and FAPbBr<sub>3</sub>, with FA being formamidinium. The SRPP data can be misinterpreted to reveal a phonon bottleneck even at low exciton concentrations, where there should be none. We circumvent that spectroscopic problem with a state-resolved method that reveals an order of magnitude faster cooling and breaking of the quantum phonon bottleneck that might be expected in nanocrystals. Since the prior pump/probe methods of analysis are shown to be ambiguous, we perform t-PL experiments to unambiguously confirm the existence of hot phonon bottlenecks as well. The t-PL experiments reveal there is no hot phonon bottleneck in these perovskite nanocrystals. Ab initio molecular dynamics simulations reproduce experiments by inclusion of efficient Auger processes. This experimental and theoretical work reveals insight on hot exciton dynamics, how they are precisely measured, and ultimately how they may be exploited in these materials.

**KEYWORDS:** perovskite, nanocrystal, quantum dot, phonon bottleneck, hot phonon bottleneck, carrier cooling

6

Time (ps)

## INTRODUCTION

Downloaded via UNIV OF SOUTHERN CALIFORNIA on March 2, 2024 at 22:06:03 (UTC). See https://pubs.acs.org/sharingguidelines for options on how to legitimately share published articles.

Metal halide perovskite nanocrystals (PNCs) have been shown to possess promising optoelectronic properties for the use in devices such as high performance solar panels and light emitting diodes. 1-4 Thus, an understanding of the fundamental behavior of photoexcited carriers is crucial for the production of efficient devices.<sup>5,6</sup> Importantly, the carrier dynamics in PNCs, have been shown to exhibit liquid-like behavior due to their dynamic, ionic lattices. <sup>7–10</sup> This liquid-like behavior results in polaron formation and protection of charge carriers from trapping. 7,11-14 The protection from trapping plays a particularly important role for hot carriers, which could be used in hot-carrier solar cells, in order to break the Shockley-Queisser limit.6,15

Received: December 8, 2022 Accepted: February 15, 2023 Published: February 16, 2023





The simple but fundamental question arises of the time scales and pathways of carrier or exciton relaxation or thermalization. The subject remains controversial for a number of reasons. Many studies on PNCs, both strongly and weakly confined, have shown that relaxation occurs on time scales of multiple picoseconds at high excitation densities. The same results are observed in perovskite films; the result is general to perovskites. These slow cooling rate constants have been attributed to an initially fast redistribution of energy, through coupling to the longitudinal optical (LO) phonon, followed by a slower process due to total occupation of this phonon mode, a phenomenon known as the "hot phonon bottleneck". Hence to this, the Auger heating processes have also been identified as a mechanism for extending hot carrier lifetimes. The point is that one expects to see hot carriers on the 10 ps time scale at high densities.

Though many studies have suggested the observation of the hot phonon bottleneck and slow cooling in PNCs; others have found much faster cooling rate constants on the order of 100s of femtoseconds in the quantum dot (QD) versions of the PNC. 22-25 In QD PNCs, the fast relaxation is attributed to processes usually associated with the electronic structure of quantum confined systems for which a "quantum phonon bottleneck" becomes relevant. In quantum confined systems such as quantum dots (QD), there are Auger energy transfer and multiphonon emission, rather than the expected bulk mechanisms, thereby breaking the quantum phonon bottleneck.<sup>24,26</sup> Furthermore, for strongly confined PNCs at low excitation densities, the observed fast carrier cooling rate constants and breaking of the quantum phonon bottleneck have been attributed to nonadiabatic coupling to surface ligands, similar to that of holes in CdSe. 27,28 A wide variety of results have emerged regarding the basic process of hot carrier thermalization in semiconductor perovskites. Hence the fundamental question of time scales and pathways of hot carrier relaxation in the model system of bulk PNC remains controversial. The basic questions remain ambiguous as to whether there is a hot phonon bottleneck under high carried densities and whether the quantum phonon bottleneck is relevant for bulk systems.

Here, we perform a suite of ultrafast spectroscopies to unambiguously unravel the presence and relevance of both hot phonon bottlenecks and quantum phonon bottlenecks. Both processes are generally evaluated using one-dimensional Transient Absorption (TA) Spectroscopy, with an arbitrary pump energy of 3.1 eV for technical expedience. In this work, we exploit state-resolved pump/probe (SRPP) with 50 fs time resolution, state-resolved time-resolved photoluminescence (t-PL) measurements with 3 ps time resolution. A simple TA analysis of two classes of PNC reveal slow electron thermalization, on the 1-10 ps time scale, even at low carrier density. In order to better unravel the TA signals, SRPP spectroscopy revealed that there is a breaking of the quantum phonon bottleneck at low carrier density. These experiments suggest that TA spectroscopy provides an ambiguous measure of carrier thermalization, especially at high carrier density where the optical nonlinearities are still poorly understood. In order to provide a direct measure of relaxation from an energetic state to the fully relaxed state, we perform time t-PL measurements over orders of magnitude in carrier density. The t-PL measurements confirm the SRPP measurements that there is a breaking of the quantum phonon bottleneck at low density. They reveal that there is also a breaking of the hot phonon bottleneck at high carrier density. The breaking of both forms of phonon bottleneck are argued to arise from Auger processes. *Ab initio* calculations with inclusion of Auger processes reproduces well the experimental results, confirming previously unobserved Auger processes in bulk perovskite nanocrystals.

## **RESULTS AND DISCUSSION**

Figure 1a shows the linear absorption spectra for CsPbBr<sub>3</sub> (red line) and FAPbBr<sub>3</sub> (blue line) as well as the pump pulse

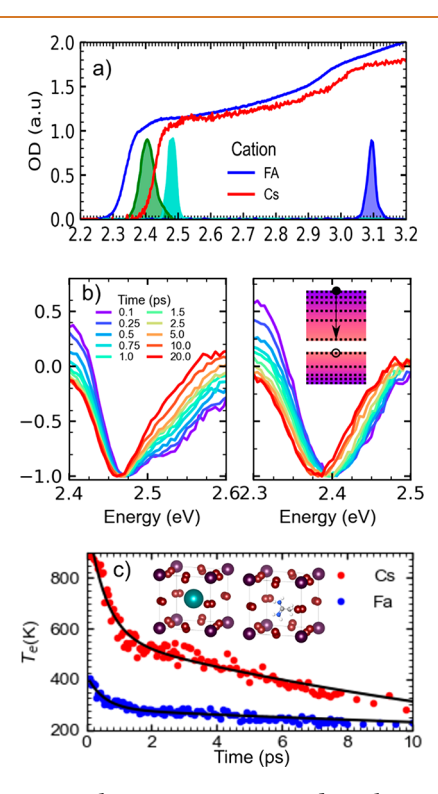


Figure 1. Linear absorption spectra and analysis of electron cooling Boltzmann fitting suggest slow carrier thermalization at low carrier densities. a) Linear absorption spectra of Bulk CsPbBr<sub>3</sub> (red) and FaPbBr<sub>3</sub> bulk NCs. Cs: 18 nm. Fa: 17 nm. Spectra for the energetic state-resolved exciting pulses are shown for both band edge (Cs, Teal; FA, Green) and continuum excitation. b) Transient absorption spectra of CsPbBr<sub>3</sub> (left) and FAPbBr<sub>3</sub> (right), excited at 3.1 eV, over a 20 ps time period. The cartoon shows electron cooling through the continuum to the band edge as indicated by the relaxation of the high energy tails in the spectra. c) Electron temperature obtained from fitting to a Boltzmann distribution for CsPbBr<sub>3</sub> (red) and FAPbBr<sub>3</sub> (blue). Black lines show a fit to a biexponential decay. Cartoons show the unit cell of CsPbBr<sub>3</sub> (left) and FAPbBr<sub>3</sub> (right). The carrier density is  $\langle N \rangle = 0.5$  per NC, corresponding to a density of  $1.5 \times 10^{17}$  cm<sup>-3</sup>.

spectra for band edge (2.40 eV green, 2.47 eV teal) and continuum (3.1 eV, blue) excitation pulses. The broad, weak peak found at the band edge for both samples is indicative of the weakly confined nature of excitons in PNCs of these sizes (Cs, 18 nm; Fa, 17 nm) where the Bohr diameter is typically 7 nm. Figure 1b shows the TA spectra for Cs (left) and FA (right) PNCs over the first 20 ps after excitation at 3.1 eV. These TA spectra both exhibit a broad, high energy tail to the band edge bleach. This broad feature is assumed to be characteristic of state-filling by hot carriers. Thus, the time dependence of this tail can in principle be used to

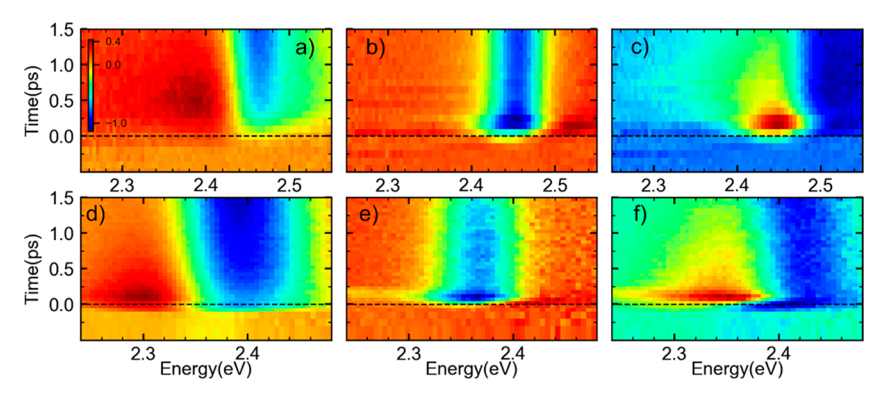


Figure 2. Energy-resolved pump/probe experiments are performed with different amounts of excess energy to compare hot carrier effects and are done simultaneously to enable careful comparison. a) Transient absorption spectrum of bulk CsPbBr<sub>3</sub> NCs with 3.1 eV excitation revealing complex dynamics within the first 1 ps. Color bar is shown for all panels. b) Transient absorption spectrum of bulk-like CsPbBr<sub>3</sub> NCs with band edge excitation. c) Transient absorption double difference spectrum ( $\Delta\Delta$ OD) of CsPbBr<sub>3</sub>. The differences are taken from spectra acquired simultaneously. d, e, f) The same as a), b), c) but for FAPbBr<sub>3</sub> NCs. The carrier density is  $\langle N \rangle = 0.5$  per NC, corresponding to a density of 1.5  $\times$  10<sup>17</sup> cm<sup>-3</sup>.

determine the rate constants of thermalization upon establishment of a quasi-equilibrium after the first 100 fs. Following the literature and as discussed in the Supporting Information, it is assumed that the tail takes the form of a Fermi–Dirac distribution, approximated to a Maxwell–Boltzmann distribution due to the large amount of excess energy supplied by the pump pulse. The results of this analysis are shown in Figure 1c for Cs (red) and Fa (blue) with the corresponding biexponential fits shown in black (full details in the Supporting Information). Both PNCs show a carrier thermalization time scale on the order of 10 ps, consistent with previous literature values using this method. 17–19,21,25,31,32 However, this method creates an initial value problem by exciting to the continuum directly; the carrier response is monitored for both the electron and hole, and the rate constant of thermalization is determined for a multitude of states and processes all convolved.

An overview of the SRPP data for both Cs (top row) and FA PNCs (bottom row) is shown in Figure 2. As noted in the Supporting Information and our other works, SRPP is merely performing two TA experiments with different pump photon energies. Importantly, these experiments are done simultaneously to minimize errors due to potential instrumental or sample instabilities. Hence the subtraction is done in real laboratory time. With band edge excitation (Figure 2b), a rapid shift in the band edge bleach position is apparent for both PNCs. This feature is completely masked upon excitation at 3.1 eV (Figure 2a,c), due to the temporal broadening from hot carriers—the initial state is not well-defined. Other features are apparent upon 3.1 eV excitation, such as a broad short-lived, photoinduced absorption (PIA) observed at lower energies compared to the band edge bleach. For the 3.1 eV pumped initial state, one sees complex spectral dynamics on the hundreds of femtoseconds time scale, especially to the red of the band edge bleach. Pumping directly into the band edge reveals qualitatively different signals. The double differential  $\Delta\Delta$ OD reveals the spectral effect of the excess energy at early time. The information within the  $\Delta\Delta$ OD signal will be discussed in further detail below.

The dynamics at two key probe energies for each sample are shown in Figure 3. Focusing initially at the band edge bleach, upon 3.1 eV excitation (blue laser spectrum in Figure 1), an attenuated bleach response is observed in both types of PNC, building up over the first picosecond after excitation. With

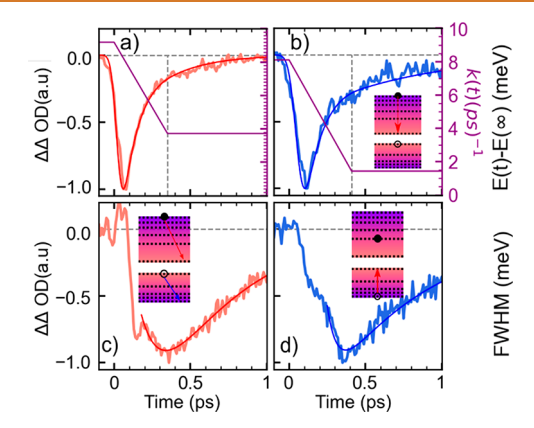


Figure 3. Time dependent survival probabilities of both electrons and holes are reflected by the  $\Delta\Delta$ OD transients, probed at the band edge bleach (electrons) and the excited state absorption subresonant to the band edge (holes). a)  $\Delta\Delta$ OD transient, representing the survival probability of electrons, in CsPbBr<sub>3</sub> (light red), fit to a varying rate constant model (dark red) and how these rate constants vary (purple line). The transients are probed at the peak of the band edge bleach as discussed in the text. Cartoon shows electron cooling. b) The same as a) but for FAPbBr<sub>3</sub>. c,d)  $\Delta\Delta$ OD transient, representing hole survival probabilities, in CsPbBr<sub>3</sub> (c, red) and FAPbBr<sub>3</sub> (d, blue). Darker lines are a biexponential fit as a guide to the eye. Transients are probed at lower energy than the band edge signal as discussed in the text. Cartoons in c,d) show initial electron cooling through Auger heating (c), followed by hole cooling (d). The carrier density is  $\langle N \rangle = 0.5$  per NC, corresponding to a density of 1.5  $\times$  $10^{17} \text{ cm}^{-3}$ .

band edge excitation (green laser spectra in Figure 1), an instrument response limited bleach is observed with a fast recovery after the first 200 fs. The difference spectra are  $\Delta\Delta$ OD in which the band edge pump signal is subtracted from the 3.1 eV pump signal to directly reveal hot carrier processes as discussed below.

To separate electronically state-to-state transitions and to disentangle carrier specific dynamics, an energetic or initial state-resolved method is required, along with suitable time—frequency resolution. Here, the energetic or quantum state (in the case of quantum dots) is controlled through subtraction of the pump—probe signal with band edge excitation from that obtained at 3.1 eV or other photon energies. Carrier specificity

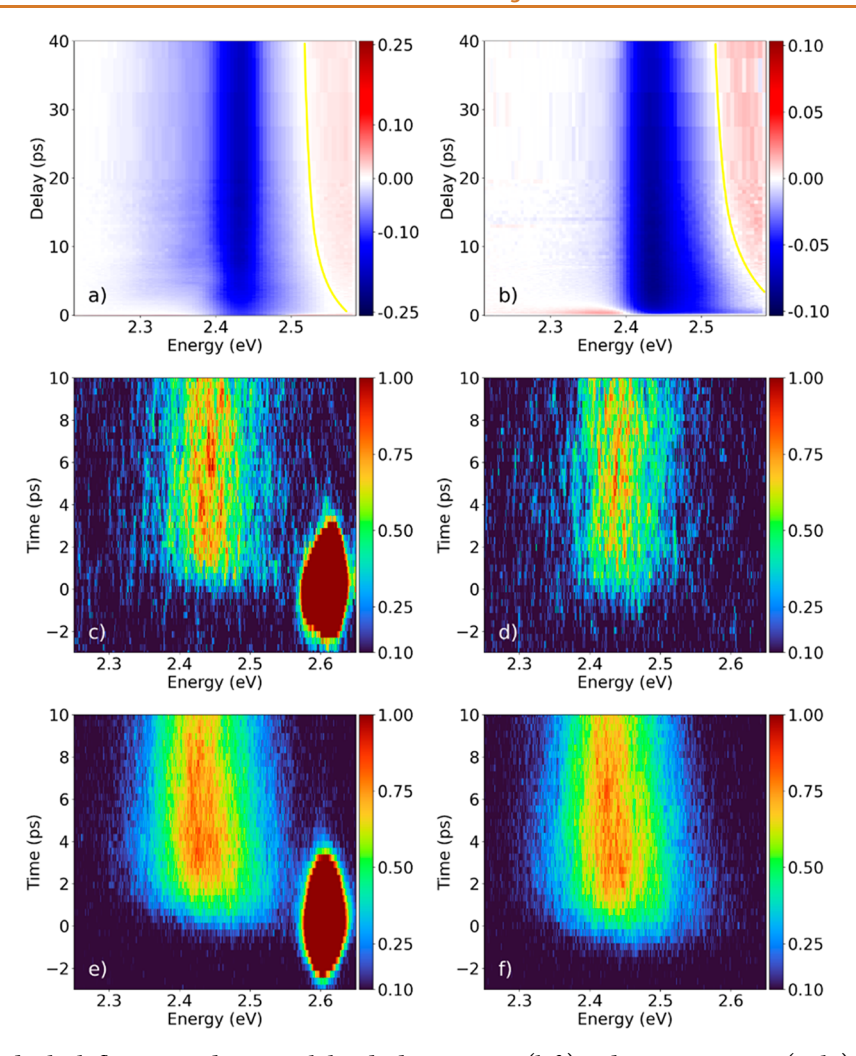


Figure 4. SRPP spectra under high fluence conditions with band edge pumping (left) and 3.1 eV pumping (right). The yellow curves are to guide the eye. Here,  $\langle N \rangle = 5$ , corresponding to a density of  $1.5 \times 10^{18}$  cm<sup>-3</sup>. t-PL spectra at low and high fluence, with energy-resolved pumping in order to directly test slow relaxation at high density. a) t-PL spectrum at low fluence with 3.1 eV pumping. Here,  $\langle N \rangle = 0.015$ , corresponding to a density of  $4.5 \times 10^{-15}$  cm<sup>-3</sup>. b) t-PL spectrum at high fluence with 3.1 eV pumping. Here,  $\langle N \rangle = 7.4$ , corresponding to a density of  $2.2 \times 10^{18}$  cm<sup>-3</sup>. c) t-PL spectrum at low fluence with 2.6 eV pumping. Here,  $\langle N \rangle = 0.017$ , corresponding to a density of  $5.1 \times 10^{15}$  cm<sup>-3</sup>. d) t-PL spectrum at high fluence with 2.6 eV pumping. Here,  $\langle N \rangle = 4.2$ , corresponding to a density of  $1.3 \times 10^{-18}$  cm<sup>-3</sup>.

in terms of electron vs hole dynamics is obtained by changing the energy at which the pump-probe (or TA) signal is monitored. Electron dynamics are reflected through monitoring of the band edge bleach signal, whereas hole dynamics are reflected in the PIA signal. 28,33,34 This method, yielding a  $\Delta\Delta$ OD transient, directly follows the difference between carriers with excess energy (hot carriers) versus those that have already completed cooled (band edge carriers). Importantly the combination of time and initially pumped state enable measurement of dynamics with 10 fs precision, thereby making this analysis possible. These transients would also be less meaningful were they to be done in series as separate experiments. As discussed above and in the Supporting Information, these experiments are done simultaneously. The resulting difference transient represents the time dependent survival probability of hot carriers, specific to either electrons or holes, based upon the probe photon energy as we have discussed in detail for CdSe quantum dots.

The  $\Delta\Delta$ OD transients for electron thermalization in Cs and FA PNCs are shown in Figure 3a,b. In both cases, the electron relaxes rapidly over a time scale of ~400 fs, qualitatively faster than the rate constant extracted from the tail fitting method.

Notably, by the first picosecond, there is almost no difference in carriers excited to the continuum and the band edge. The time scales upon which this process occurs are an order of magnitude faster than those extracted from the tail fitting method shown in Figure 1, indicating the absence of a quantum phonon bottleneck in these materials which might show quantum confinement effects, whether due to static structure or due to structural dynamics. This observation of a breaking of the expected phonon bottleneck raises the question of the mechanism given these are bulk NC. But unlike prior NC such as CdSe which are covalent, these PNC are ionic and undergo complex structural dynamics akin to a glass.

In order to glean further insight into the mechanism, we present both fitting and modeling, as discussed in detail in the Supporting Information. Qualitatively, these data take a biexponential form, with an initially fast time scale of  $\sim$ 400 fs (1/e), followed by a slower time scale of  $\sim$ 1 ps. However, on fitting with this model, large deviations are found in the residuals, making this model unsuitable. Moreover, this model is nonphysical even if it were to accurately reproduce the data. There is no reason for the excited state population to undergo

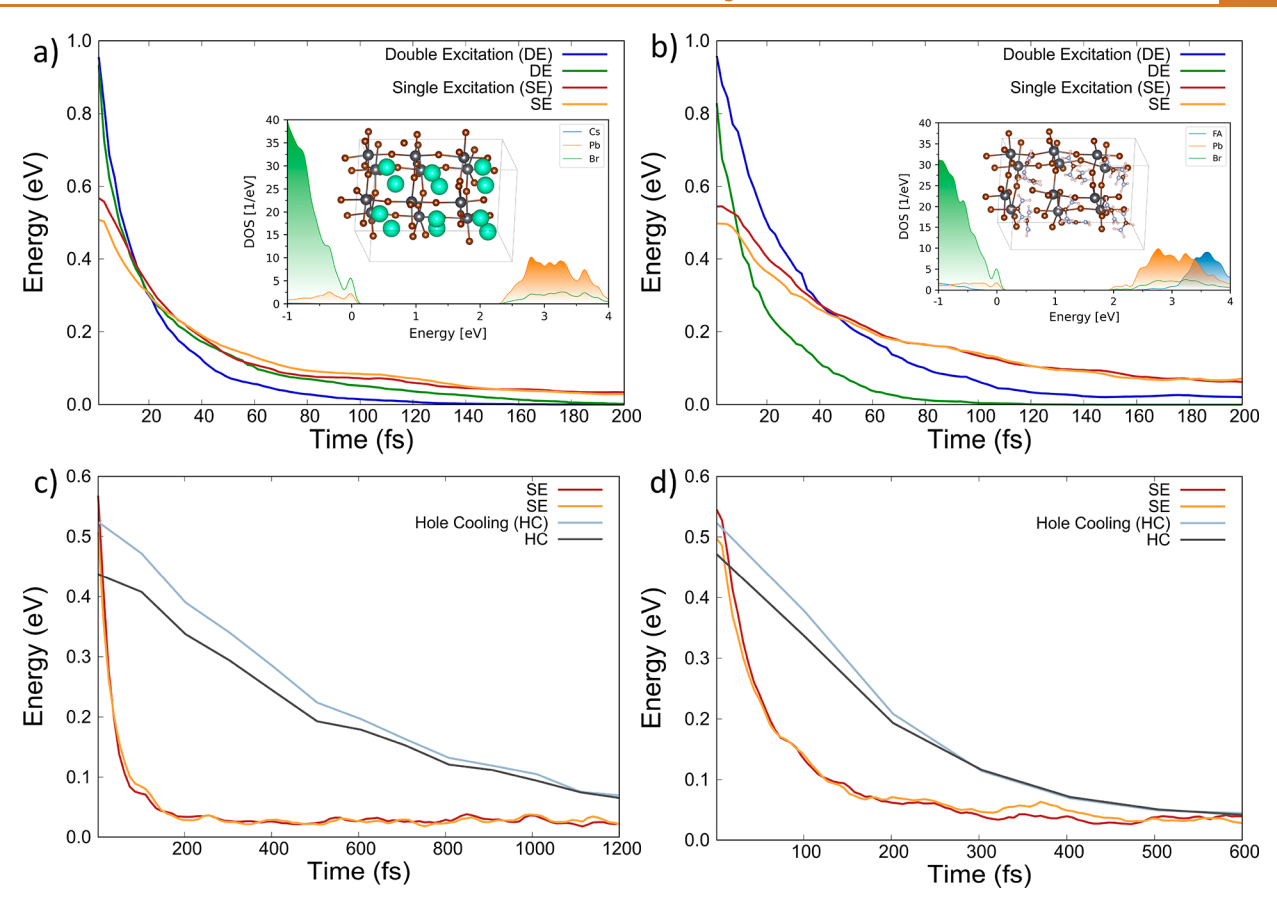


Figure 5. Comparison of electron cooling for single (SE) and double (DE) electron excitations in a) CsPbBr<sub>3</sub> and b) FAPbBr<sub>3</sub>. DEs are slightly faster than SEs because DEs have more channels for energy relaxation. The canonically averaged DOS is included for each system, together with a structure cell. Charge densities of the band edge and excitation orbitals are shown in Figure S5. Comparison of electron SE and hole cooling (HC) for c) CsPbBr<sub>3</sub> and d) FAPbBr<sub>3</sub>. The simulated time scales agree with the experimental results, Figure 3.

nonexponential dynamics if simple kinetics were to hold, as in the case of CdSe quantum dots.

Relaxation from the continuum occurs through a complex set of channels, including occupation of phonon modes and Auger processes, following quantum dynamics. Here a simple model is proposed to describe these complex processes; the initial relaxation of the electron occurs through a dense manifold of states in the continuum, which becomes sparser as the electron approaches the band edge. Full details of this model can be found in the Supporting Information. It is noted that other models have been proposed in the literature.<sup>35,36</sup> This quantum dynamic model returns the qualitative nonexponential behavior of the experimental data, in both cases, an initially fast rate constant, decaying rapidly over ~400 fs, the time scale of polaron formation, followed by a slower rate constant after this time. More important than the quality of the fit is that the quantum dynamical model rationalizes the observations in terms of theory that can be tested.

Comparing Cs to FA, cooling occurs more rapidly for the inorganic cation, inconsistent with previous, cation dependent, studies. <sup>25,32,37-40</sup> This relates to the different hole cooling rate constants observed for the different cations. Here, we propose that the previous observations of slow cooling of electrons in PNCs are instead the late time cooling of the holes. Thus, the faster rate constants observed for organic cations versus inorganic relate instead to their hole cooling rate constants. These results which suggest the cation has little effect on the exciton dynamics is on the other hand, consistent with the idea

that the octahedral cages are more important to the structural dynamics which give rise to the carrier dynamics.

Further evidence of quantum effects arising during the course of the relaxation process can be seen in the hole dynamics shown in Figure 3c,d. The idea is that the initially absorbing state is bulk-like or weakly quantum confined but dynamically evolves into a more strongly confined system which supports quantum dot physics. With this idea of examining the carrier cooling dynamics for quantum confinement effects, the aim spectroscopically is to see if there is some electron-to-hole type of energy transfer process that might be resolvable by a buildup in a hole signal. In both cases, a rise time of ~200 fs is observed, followed by a slower cooling process on the 1 ps time scale. The growth observed is a signature of electron-hole energy transfer through intraband Auger relaxation as is seen in traditional II-VI semiconducting NCs such as CdSe, followed by a phonon mediated cooling process. 28,41,42 Different from CdSe and other semiconducting nanocrystals, PNCs show a delay before the onset of hole heating through Auger processes, beginning roughly 200 fs after photoexcitation due to these quantum confinement induced cooling paths arising in time due to the complex glassy structural dynamics in PNC.

In order to evaluate the hot phonon bottleneck that is more commonly discussed in perovskites than the quantum phonon bottleneck, we perform experiments at high carrier concentration as well. In the case of both bottlenecks, they are different in physics but were supported by early experiments and rationalized in terms of bulk semiconductor physics. Both have been implicated to be of importance in NC based photovoltaics by aiming to find slow carrier cooling.

Figure 4 shows the SRPP data and t-PL data with both band edge pumping and 3.1 eV pumping at high excitation densities in which hot phonon bottlenecks are expected to arise in perovskites. In the low density case  $\langle N \rangle = 0.5$ , whereas in the high density cases  $\langle N \rangle = 5$ , corresponding to a density of 1.5  $\times$ 10<sup>18</sup> cm<sup>-3</sup>. The SRPP measurements at high fluence indeed reveal dynamics on the 1-10 ps time scale. The same time scale dynamics are seen with direct band edge pumping into cold carriers with no excess energy. If the 1–10 ps dynamics in TA measurements are due to hot carrier cooling, then why is there the same cooling process when there is no excess energy and the carriers are fully cold? These experiments reveal that there are complexities in the nonlinear spectroscopy of perovskite NC which need to be better understood and are currently obfuscating critical evaluation of the hot phonon bottleneck.

In order to directly measure the presence of hot carriers at high concentration, we perform t-PL measurements with 3 ps time resolution and selective pumping into both the band edge and at 3.1 eV. At low carrier concentrations of  $\langle N \rangle < 1$ , there is no hot PL observed at either pump photon energy. At high carrier concentrations of  $\langle N \rangle \sim >5$ , once again there is no hot PL observed. Since the time resolution of the t-PL is 3 ps, the 10 ps dynamics in TA experiments should be easily visible. With this time resolution, even 1 ps hot PL should be observable, albeit within the instrument response function. The complete absence of hot PL at 3.1 eV pump at high carrier density is conclusive proof that there is no hot phonon bottleneck in these bulk perovskite NC.

In order to rationalize these experimental results at the atomistic level, we perform ab initio quantum dynamics calculations, as detailed in the Supporting Information. We investigate the impact of Auger and electron-vibrational relaxation processes on the electron cooling in CsPbBr3 and FAPbBr<sub>3</sub>. The modeled systems are composed of  $2 \times 2 \times 3$ supercells containing 12 formula units of APbBr3 (A = Cs or FA) as shown in the insets of Figure 5. The density of states (DOS) of both systems is asymmetric, with the valence band (VB) rising faster than the conduction band (CB). This indicates that the pump energy is distributed unevenly between electrons and holes, with electrons gaining more energy than holes because there are more hole states close to the band edge. Subsequently, the energy is transferred from electrons to holes via the Auger mechanism. The higher VB DOS also indicates that energy spacings are smaller in the VB than in the CB, and hence, the nonadiabatic coupling (NAC) is stronger for holes than for electrons, as shown in Figure S8. The stronger NAC results in faster hole-vibrational relaxation than electron-vibrational relaxation, as established previously.<sup>37,43-46</sup> Finally, the DOS is slightly higher in CsPbBr<sub>3</sub> than in FAPbBr<sub>3</sub>, in particular in the VB. The higher VB DOS provides a larger density of hole states, accelerating Auger energy transfer from electrons to holes in CsPbBr3 relative to FAPbBr<sub>3</sub>.

Figure 5a,b presents relaxation of electrons in CsPbBr<sub>3</sub> and FAPbBr<sub>3</sub>, following either a single excitation (SE) or a double excitation (DE). Two representative initial conditions are chosen in each case. Auger energy transfer from electrons to holes, and electron-vibrational relaxation takes place simultaneously. However, the Auger mechanism dominates, resulting

in sub-100 fs relaxation time scales. The relaxation is faster in CsPbBr3 than in FAPbBr3 because of the higher VB DOS in the former. The calculated time scales agree with the experimental data, Figure 3a,b, and are somewhat faster, because the simulated systems are small due to computational limitations, the charges are close to each other, and the Coulomb interactions are enhanced. The relaxation of electrons purely due to coupling to phonons occurs on a much longer, picosecond time scale, as established in the earlier calculations. 37,43-46 Figure 5a,b shows relaxation of electrons following a double excitation (DE) as well. The relaxation is also dominated by energy transfer to holes rather than by the electron-vibrational mechanism. Notably, the relaxation of electrons following a DE proceeds on the same time scale and even slightly faster than the relaxation following a SE, and no phonon bottleneck is observed. The DE leads to a slightly faster relaxation than the SE because of a larger number of relaxation pathways available with two excited electrons. Finally, Figure 5c,d presents hole cooling (HC) due to coupling to phonons. The HC takes several hundred femtoseconds and is slightly faster in CsPbBr<sub>3</sub> than in FAPbBr<sub>3</sub> due to a higher VB DOS and stronger NAC, Figure S8. This is in agreement with the experimental results, Figure 3c,d, and the prior quantum dynamics calculations. <sup>37,43–46</sup>

#### **CONCLUSIONS**

In summary, state-resolved pump/probe spectroscopy and time-resolved PL were performed on two classes of bulk-like perovskite nanocrystals which reveal qualitatively different behavior from the past decade of literature. The pump/probe spectroscopy at low exciton concentration reveals a breaking of the quantum phonon bottleneck via electron to hole energy transfer that is missed in generic transient absorption analysis. The pump/probe spectroscopy at high exciton concentration can be interpreted as revealing a hot phonon bottleneck, but the signals were misinterpreted in the past. Even pumping with zero excess energy gives the illusion of a hot exciton bottleneck. Hence t-PL experiments were performed to unambiguously resolve the time scale of energy dissipation. The t-PL measurements conclusively show that there is no hot phonon bottleneck in these bulk perovskite NCs. The ambiguities in transient absorptive experiments vs the clarity of transient emissive experiments has also recently been revealed by photoelectron spectroscopy by Chergui. 47,48 Finally, ab initio molecular dynamics rationalizes the experimental observation in light of efficient Auger processes. These experiments provide an accurate view of hot exciton processes in perovskites which can be exploited to advance their use in optoelectronic devices which are related to hot exciton thermalization processes.

## **EXPERIMENT**

The state-resolved pump/probe (SRPP) measurements reported here are performed wherein two pumped energy states are simultaneously measured to minimize errors due to sample evolving or photoproducts or instrumental drift. The instrument response function (IRF) of 50 fs is consistent across all analyzed energies, with all spectra and transients collected simultaneously for both pump energies. Energetic state-resolved pumping is employed. Samples of CsPbBr $_3$  and FAPbBr $_3$  are dispersed in toluene and flowed at 298 K through a 1 mm quartz flow cell using a peristaltic pump. Pump fluences remained constant at 75 nJ/pulse for all pump energies. A pump fluence of 75 nJ/pulse was selected in both cases in order to remain in the regime where the average excitation per NC is 0.5 for

low fluence measurements. High fluence measurements were performed with  $\langle N \rangle = 5$ . Time-resolved photoluminescence (t-PL) spectroscopy was performed using an optically triggered streak camera with a 3 ps IRF, and energy-resolved pumping. The t-PL measurements were conducted from  $N \sim 0.01$  to 7. The exciton density of  $\langle N \rangle = 1$  per NC corresponds to a density of  $2 \times 10^{17}$  cm $^{-3}$ . Full details of all spectroscopies and materials synthesis and characterization can be found in the Supporting Information.

#### **ASSOCIATED CONTENT**

# **Supporting Information**

The Supporting Information is available free of charge at https://pubs.acs.org/doi/10.1021/acsnano.2c12220.

Synthetic and experimental details, experimental details for SRPP, t-PL spectroscopies, and modeling, TEM images, Maxwell—Boltzmann fitting, instrument response functions and Gaussian fits, canonically averaged projected density of states, canonically averaged charge densities, DOS, canonically averaged absolute non-adiabatic coupling (PDF)

## **AUTHOR INFORMATION**

#### **Corresponding Author**

Patanjali Kambhampati — Department of Chemistry, McGill University, Montreal, Quebec H3A 0B8, Canada; orcid.org/0000-0003-0146-3544; Phone: +1-514-398-

7228; Email: pat.kambhampati@mcgill.ca

#### **Authors**

Harry Baker – Department of Chemistry, McGill University, Montreal, Quebec H3A 0B8, Canada

Carlos Mora Perez – Department of Chemistry, University of Southern California, Los Angeles, California 90089, United States

Colin Sonnichsen – Department of Chemistry, McGill University, Montreal, Quebec H3A 0B8, Canada

Dallas Strandell – Department of Chemistry, McGill University, Montreal, Quebec H3A 0B8, Canada

Oleg V. Prezhdo – Department of Chemistry, University of Southern California, Los Angeles, California 90089, United States; © orcid.org/0000-0002-5140-7500

Complete contact information is available at: https://pubs.acs.org/10.1021/acsnano.2c12220

## **Author Contributions**

Experiments and analysis were done by H. Baker, C. Sonnichsen, and D. Strandell. Calculations were done by C. Mora Perez and O. V. Prezhdo. Materials were synthesized and characterized by D. Strandell. The manuscript was written by H. Baker, C. Mora Perez, O. V. Prezhdo, and P. Kambhampati. P. Kambhampati supervised the work.

## **Funding**

P.K. acknowledges financial support from NSERC, CFI, FQRNT, Sony Corporation, and McGill University is acknowledged. O.V.P. acknowledges support of the US National Science Foundation, grant CHE-2154367.

#### Notes

The authors declare no competing financial interest.

# **REFERENCES**

(1) Protesescu, L.; Yakunin, S.; Bodnarchuk, M. I.; Krieg, F.; Caputo, R.; Hendon, C. H.; Yang, R. X.; Walsh, A.; Kovalenko, M. V. Nanocrystals of Cesium Lead Halide Perovskites (CsPbX3, X = Cl,

- Br, and I): Novel Optoelectronic Materials Showing Bright Emission with Wide Color Gamut. *Nano Lett.* **2015**, *15* (6), 3692–3696.
- (2) Kovalenko, M. V.; Protesescu, L.; Bodnarchuk, M. I. Properties and Potential Optoelectronic Applications of Lead Halide Perovskite Nanocrystals. *Science* **2017**, *358* (6364), 745–750.
- (3) Fu, Y.; Zhu, H.; Chen, J.; Hautzinger, M. P.; Zhu, X. Y.; Jin, S. Metal Halide Perovskite Nanostructures for Optoelectronic Applications and the Study of Physical Properties. *Nat. Rev. Mater.* **2019**, 4 (3), 169–188.
- (4) Manser, J. S.; Christians, J. A.; Kamat, P. V. Intriguing Optoelectronic Properties of Metal Halide Perovskites. *Chem. Rev.* **2016**, *116* (21), 12956–13008.
- (5) Zhu, C.; Niu, X.; Fu, Y.; Li, N.; Hu, C.; Chen, Y.; He, X.; Na, G.; Liu, P.; Zai, H.; Ge, Y.; Lu, Y.; Ke, X.; Bai, Y.; Yang, S.; Chen, P.; Li, Y.; Sui, M.; Zhang, L.; Zhou, H.; Chen, Q. Strain Engineering in Perovskite Solar Cells and Its Impacts on Carrier Dynamics. *Nat. Commun.* 2019, 10 (1), 815.
- (6) Kahmann, S.; Loi, M. A. Hot Carrier Solar Cells and the Potential of Perovskites for Breaking the Shockley-Queisser Limit. *J. Mater. Chem. C* **2019**, 7 (9), 2471–2486.
- (7) Miyata, K.; Atallah, T. L.; Zhu, X. Y. Lead Halide Perovskites: Crystal-Liquid Duality, Phonon Glass Electron Crystals, and Large Polaron Formation. *Sci. Adv.* **2017**, 3 (10), 1–11.
- (8) Seiler, H.; Palato, S.; Sonnichsen, C.; Baker, H.; Socie, E.; Strandell, D. P.; Kambhampati, P. Two-Dimensional Electronic Spectroscopy Reveals Liquid-like Lineshape Dynamics in CsPbI3 Perovskite Nanocrystals. *Nat. Commun.* **2019**, *10* (1), 1–8.
- (9) Guo, Y.; Yaffe, O.; Hull, T. D.; Owen, J. S.; Reichman, D. R.; Brus, L. E. Dynamic Emission Stokes Shift and Liquid-like Dielectric Solvation of Band Edge Carriers in Lead-Halide Perovskites. *Nat. Commun.* **2019**, *10* (1), 1–8.
- (10) Yaffe, O.; Guo, Y.; Tan, L. Z.; Egger, D. A.; Hull, T.; Stoumpos, C. C.; Zheng, F.; Heinz, T. F.; Kronik, L.; Kanatzidis, M. G.; Owen, J. S.; Rappe, A. M.; Pimenta, M. A.; Brus, L. E. Local Polar Fluctuations in Lead Halide Perovskite Crystals. *Phys. Rev. Lett.* **2017**, *118*, 136001.
- (11) Park, M.; Neukirch, A. J.; Reyes-Lillo, S. E.; Lai, M.; Ellis, S. R.; Dietze, D.; Neaton, J. B.; Yang, P.; Tretiak, S.; Mathies, R. A. Excited-State Vibrational Dynamics toward the Polaron in Methylammonium Lead Iodide Perovskite. *Nat. Commun.* **2018**, *9* (1), 1–9.
- (12) Thouin, F.; Valverde-Chávez, D. A.; Quarti, C.; Cortecchia, D.; Bargigia, I.; Beljonne, D.; Petrozza, A.; Silva, C.; Srimath Kandada, A. R. Phonon Coherences Reveal the Polaronic Character of Excitons in Two-Dimensional Lead Halide Perovskites. *Nat. Mater.* **2019**, *18* (4), 349–356.
- (13) Evans, T. J. S.; Miyata, K.; Joshi, P. P.; Maehrlein, S.; Liu, F.; Zhu, X. Y. Competition between Hot-Electron Cooling and Large Polaron Screening in CsPbBr3 Perovskite Single Crystals. *J. Phys. Chem. C* 2018, 122 (25), 13724–13730.
- (14) Wang, F.; Fu, Y.; Ziffer, M. E.; Dai, Y.; Maehrlein, S. F.; Zhu, X. Y. Solvated Electrons in Solids Ferroelectric Large Polarons in Lead Halide Perovskites. *J. Am. Chem. Soc.* **2021**, *143* (1), 5–16.
- (15) Ross, R. T.; Nozik, A. J. Efficiency of Hot-Carrier Solar Energy Converters. *J. Appl. Phys.* **1982**, *53* (5), 3813–3818.
- (16) Li, M.; Bhaumik, S.; Goh, T. W.; Kumar, M. S.; Yantara, N.; Grätzel, M.; Mhaisalkar, S.; Mathews, N.; Sum, T. C. Slow Cooling and Highly Efficient Extraction of Hot Carriers in Colloidal Perovskite Nanocrystals. *Nat. Commun.* **2017**, 8 (May), 14350.
- (17) Fu, J.; Xu, Q.; Han, G.; Wu, B.; Huan, C. H. A.; Leek, M. L.; Sum, T. C. Hot Carrier Cooling Mechanisms in Halide Perovskites. *Nat. Commun.* **2017**, 8 (1), 1300.
- (18) Li, M.; Fu, J.; Xu, Q.; Sum, T. C. Slow Hot-Carrier Cooling in Halide Perovskites: Prospects for Hot-Carrier Solar Cells. *Adv. Mater.* **2019**, *31* (47), 1802486.
- (19) Shen, Q.; Ripolles, T. S.; Even, J.; Ogomi, Y.; Nishinaka, K.; Izuishi, T.; Nakazawa, N.; Zhang, Y.; Ding, C.; Liu, F.; Toyoda, T.; Yoshino, K.; Minemoto, T.; Katayama, K.; Hayase, S. Slow Hot Carrier Cooling in Cesium Lead Iodide Perovskites. *Appl. Phys. Lett.* **2017**, *111* (15), 153903.

- (20) Savill, K. J.; Klug, M. T.; Milot, R. L.; Snaith, H. J.; Herz, L. M. Charge-Carrier Cooling and Polarization Memory Loss in Formamidinium Tin Triiodide. *J. Phys. Chem. Lett.* **2019**, *10* (20), 6038–6047.
- (21) Papagiorgis, P.; Protesescu, L.; Kovalenko, M. V.; Othonos, A.; Itskos, G. Long-Lived Hot Carriers in Formamidinium Lead Iodide Nanocrystals. *J. Phys. Chem. C* **2017**, *121* (22), 12434–12440.
- (22) Chung, H.; Jung, S. Il; Kim, H. J.; Cha, W.; Sim, E.; Kim, D.; Koh, W.-K.; Kim, J. Composition-Dependent Hot Carrier Relaxation Dynamics in Cesium Lead Halide (CsPbX 3, X = Br and I) Perovskite Nanocrystals. *Angew. Chem.* **2017**, *129* (15), 4224–4228.
- (23) Mondal, A.; Aneesh, J.; Kumar Ravi, V.; Sharma, R.; Mir, W. J.; Beard, M. C.; Nag, A.; Adarsh, K. V. Ultrafast Exciton Many-Body Interactions and Hot-Phonon Bottleneck in Colloidal Cesium Lead Halide Perovskite Nanocrystals. *Phys. Rev. B* **2018**, *98* (11), 1–8.
- (24) Makarov, N. S.; Guo, S.; Isaienko, O.; Liu, W.; Robel, I.; Klimov, V. I. Spectral and Dynamical Properties of Single Excitons, Biexcitons, and Trions in Cesium-Lead-Halide Perovskite Quantum Dots. *Nano Lett.* **2016**, *16* (4), 2349–2362.
- (25) Chen, J.; Messing, M. E.; Zheng, K.; Pullerits, T. Cation-Dependent Hot Carrier Cooling in Halide Perovskite Nanocrystals. *J. Am. Chem. Soc.* **2019**, *141* (8), 3532–3540.
- (26) Schaller, R. D.; Pietryga, J. M.; Goupalov, S. V.; Petruska, M. A.; Ivanov, S. A.; Klimov, V. I. Breaking the Phonon Bottleneck in Semiconductor Nanocrystals via Multiphonon Emission Induced by Intrinsic Nonadiabatic Interactions. *Phys. Rev. Lett.* **2005**, *95* (19), 1–4
- (27) Li, Y.; Lai, R.; Luo, X.; Liu, X.; Ding, T.; Lu, X.; Wu, K. On the Absence of a Phonon Bottleneck in Strongly Confined CsPbBr3 Perovskite Nanocrystals. *Chem. Sci.* **2019**, *10* (23), 5983–5989.
- (28) Cooney, R. R.; Sewall, S. L.; Anderson, K. E. H.; Dias, E. A.; Kambhampati, P. Breaking the Phonon Bottleneck for Holes in Semiconductor Quantum Dots. *Phys. Rev. Lett.* **2007**, 98 (17), 1–4.
- (29) Yang, Y.; Ostrowski, D. P.; France, R. M.; Zhu, K.; Van De Lagemaat, J.; Luther, J. M.; Beard, M. C. Observation of a Hot-Phonon Bottleneck in Lead-Iodide Perovskites. *Nat. Photonics* **2016**, *10* (1), 53–59.
- (30) Nie, Z.; Gao, X.; Ren, Y.; Xia, S.; Wang, Y.; Shi, Y.; Zhao, J.; Wang, Y. Harnessing Hot Phonon Bottleneck in Metal Halide Perovskite Nanocrystals via Interfacial Electron-Phonon Coupling. *Nano Lett.* **2020**, 20 (6), 4610–4617.
- (31) Herz, L. M. Charge-Carrier Dynamics in Organic-Inorganic Metal Halide Perovskites. *Annu. Rev. Phys. Chem.* **2016**, 67 (February), 65–89.
- (32) Hopper, T. R.; Gorodetsky, A.; Frost, J. M.; Müller, C.; Lovrincic, R.; Bakulin, A. A. Ultrafast Intraband Spectroscopy of Hot-Carrier Cooling in Lead-Halide Perovskites. *ACS Energy Lett.* **2018**, 3 (9), 2199–2205.
- (33) Kambhampati, P. Unraveling the Ttructure and Dynamics of Excitons in Semiconductor Quantum Dots. *Acc. Chem. Res.* **2011**, *44* (1), 1–13.
- (34) Kambhampati, P. Hot Exciton Relaxation Dynamics in Semiconductor Quantum Dots: Radiationless Transitions on the Nanoscale Hot Exciton Relaxation Dynamics in Semiconductor Quantum Dots: Radiationless Transitions on the Nanoscale. Patanjali Kambhampati \*. J. Phys. Chem. C 2011, 115, 22089–22109.
- (35) Boehme, S. C.; ten Brinck, S.; Maes, J.; Yazdani, N.; Zapata, F.; Chen, K.; Wood, V.; Hodgkiss, J. M.; Hens, Z.; Geiregat, P.; Infante, I. Phonon-Mediated and Weakly Size-Dependent Electron and Hole Cooling in CsPbBr3 Nanocrystals Revealed by Atomistic Simulations and Ultrafast Spectroscopy. *Nano Lett.* **2020**, *20* (3), 1819–1829.
- (36) Forde, A.; Inerbaev, T.; Hobbie, E. K.; Kilin, D. S. Excited-State Dynamics of a CsPbBr3 Nanocrystal Terminated with Binary Ligands: Sparse Density of States with Giant Spin-Orbit Coupling Suppresses Carrier Cooling. *J. Am. Chem. Soc.* **2019**, *141* (10), 4388–4397.
- (37) Madjet, M. E.; Berdiyorov, G. R.; El-Mellouhi, F.; Alharbi, F. H.; Akimov, A. V.; Kais, S. Cation Effect on Hot Carrier Cooling in

- Halide Perovskite Materials. J. Phys. Chem. Lett. 2017, 8 (18), 4439-
- (38) Wang, T.; Daiber, B.; Frost, J. M.; Mann, S. A.; Garnett, E. C.; Walsh, A.; Ehrler, B. Indirect to Direct Bandgap Transition in Methylammonium Lead Halide Perovskite. *Energy Environ. Sci.* **2017**, 10 (2), 509–515.
- (39) Bokdam, M.; Sander, T.; Stroppa, A.; Picozzi, S.; Sarma, D. D.; Franchini, C.; Kresse, G. Role of Polar Phonons in the Photo Excited State of Metal Halide Perovskites. *Sci. Rep.* **2016**, *6*, 1–8.
- (40) Batignani, G.; Fumero, G.; Srimath Kandada, A. R.; Cerullo, G.; Gandini, M.; Ferrante, C.; Petrozza, A.; Scopigno, T. Probing Femtosecond Lattice Displacement upon Photo-Carrier Generation in Lead Halide Perovskite. *Nat. Commun.* **2018**, *9* (1), 1–5.
- (41) An, J. M.; Franceschetti, A.; Dudiy, S. V.; Zunger, A. The Peculiar Electronic Structure of PbSe Quantum Dots. *Nano Lett.* **2006**, *6* (12), 2728–2735.
- (42) Cooney, R. R.; Sewall, S. L.; Dias, E. A.; Sagar, D. M.; Anderson, K. E. H.; Kambhampati, P. Unified Picture of Electron and Hole Relaxation Pathways in Semiconductor Quantum Dots. *Phys. Rev. B Condens. Matter Mater. Phys.* **2007**, 75 (24), 1–14.
- (43) Li, W.; Zhou, L.; Prezhdo, O. V.; Akimov, A. V. Spin-Orbit Interactions Greatly Accelerate Nonradiative Dynamics in Lead Halide Perovskites. *ACS Energy Lett.* **2018**, 3 (9), 2159–2166.
- (44) Liu, Q.; Li, A.; Chu, W.; Prezhdo, O. V.; Liang, W. Influence of Intrinsic Defects on the Structure and Dynamics of the Mixed Pb-Sn Perovskite: First-Principles DFT and NAMD Simulations. *J. Mater. Chem. A* **2021**, *10* (1), 234–244.
- (45) Ghosh, D.; Perez, C. M.; Prezhdo, O.; Nie, W.; Tretiak, S.; Neukirch, A. J. Impact of Composition Engineering on Charge Carrier Cooling in Hybrid Perovskites: Computational Insights. *J. Mater. Chem. C* **2022**, *10*, 9563.
- (46) Hedley, G. J.; Quarti, C.; Harwell, J.; Prezhdo, O. V.; Beljonne, D.; Samuel, I. D. W. Hot-Hole Cooling Controls the Initial Ultrafast Relaxation in Methylammonium Lead Iodide Perovskite. *Sci. Rep.* **2018**, *8* (1), 8115.
- (47) Polishchuk, S.; Puppin, M.; Crepaldi, A.; Gatti, G.; Dirin, D. N.; Nazarenko, O.; Colonna, N.; Marzari, N.; Kovalenko, M. V.; Grioni, M.; Chergui, M. Nanoscale-Resolved Surface-to-Bulk Electron Transport in CsPbBr3 Perovskite. *Nano Lett.* **2022**, 22 (3), 1067–1074.
- (48) Puppin, M.; et al. Evidence of Large Polarons in Photoemission Band Mapping of the Perovskite Semiconductor CsPbBr. *Phys. Rev. Lett.* **2020**, *124*, 206402.